

The Double-Ellipsoid Geometry of CLIP

Meir Yossef Levi, Guy Gilboa

Viterbi Faculty of Electrical and Computer Engineering
Technion - Israel Institute of Technology, Haifa, Israel

me.levi@campus.technion.ac.il ; guy.gilboa@ee.technion.ac.il

Abstract

Contrastive Language-Image Pre-Training (CLIP) is highly instrumental in machine learning applications within a large variety of domains. We investigate the geometry of this embedding, which is still not well understood. We examine the raw unnormalized embedding and show that text and image reside on linearly separable ellipsoid shells, not centered at the origin. We explain the benefits of having this structure, allowing to better embed instances according to their uncertainty during contrastive training. Frequent concepts in the dataset yield more false negatives, inducing greater uncertainty. A new notion of conformity is introduced, which measures the average cosine similarity of an instance to any other instance within a representative data set. We show this measure can be accurately estimated by simply computing the cosine similarity to the modality mean vector. Furthermore, we find that CLIP’s modality gap optimizes the matching of the conformity distributions of image and text.

1. Introduction

Multi-modal approaches, particularly Contrastive Language-Image Pre-Training (CLIP) [44], have significantly advanced various computer vision tasks, enabling applications that were hard to imagine just a few years ago. These advancements include generating high-quality images from user prompts [41, 45]; performing open-vocabulary classification [18], segmentation [34, 57] and detection [54]; captioning [7, 40], and even semantic editing [27, 29]. Much of this success can be attributed to the key advancements made in multi-modal learning, with CLIP playing a key role. Following the remarkable success of vision-language models (VLMs), a wide range of adaptations has emerged for additional domains such as 3D [5, 19, 58], video [37, 49] and audio [15, 53].

Despite the practical advances, the structure of CLIP’s latent space is not fully understood. While properties such as alignment, uniformity, and the well-studied modality gap

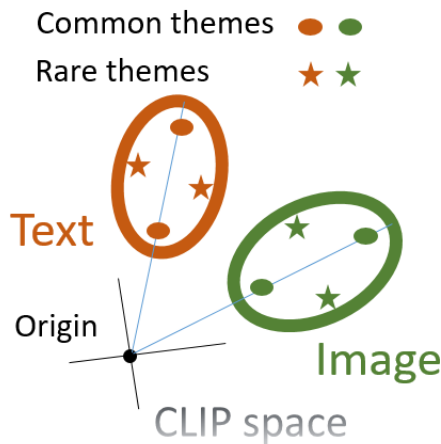


Figure 1. Sketch of CLIP general geometry: image and text are embedded on linearly separable ellipsoid shells, not centered at the origin. This allows to control uncertainty in contrastive learning, where as themes become more rare (lower uncertainty) they reside farther from the mean modality vector.

have been explored, they do not fully capture the geometry underlying this multi-modal space. A common approach is to investigate the geometry of the raw embedding after projection to the unit hypersphere. It was thus argued that CLIP features lie on a low aperture cone [35]. Since projection is an information reducing operation which “flattens” the data, we examine the raw embedding, before normalization to a unit norm. We show that CLIP’s raw latent space exhibits a double-ellipsoid geometry, one for text and one for images. Both ellipsoids are shifted from the origin (see Fig. 1). The offset from the origin explains the *narrow cone effect*, while their separability explains the *modality gap* phenomenon [11, 35, 47].

We perform a data-driven analysis of CLIP’s latent space using the MS COCO [36] validation set, without relying on any prior assumptions. We observe that both distributions of image and text follow the thin shell phenomenon [31, 32], typical of high dimensional data, in which most of the mass concentrates within some range from the mean.

We then examine the afforded advantages of this geometry. It is shown that shifting the mass from the origin allows to control the sharpness of the response in contrastive learning. A known phenomenon in unsupervised contrastive learning is the existence of false negatives [3, 33, 56]. That is, negative instances in the batch possessing similar concepts which should not be embedded far apart. False negatives can considerably degrade performance [4, 22]. This can be mitigated to some extent by reducing the sharpness of the response. Thus, as uncertainty grows the network produces a more “blurred” response, reducing the overall loss for the entire dataset. We refer to this as *semantic blurring*. Practically, this is done by embedding uncertain concepts closer (in terms of cosine distance) to the mean vector. Uncertainty grows as the concept is more frequent, with higher probability of false negatives in the batch. We thus predict that frequent concepts are better aligned to the mean vector of the ellipsoid. We validate this experimentally achieving excellent agreement with our hypothesis. Finally, we suggest a new way for image interpolation afforded by the deeper understanding of the geometry. Our contributions can be summarized as follows:

1. We investigate the raw CLIP embedding showing each modality resides on a separable ellipsoid shell not centered at the origin.
2. We analyze the advantages of such structure, allowing to control the sharpness of the response in contrastive learning.
3. False negative cases are shown to benefit mostly from this embedding. We demonstrate that the contrastive loss is optimized near CLIP’s ellipsoid offsets, for the MS-COCO dataset.
4. A new definition of concept *conformity* is proposed, quantifying the popularity of a concept. We find that conformity is correlated to (cosine) similarity to the mean vector with a remarkable Pearson correlation of 0.9998 (for both image and text on MS-COCO).
5. We reveal that the distribution of the conformity of image and text are different and are best matched in CLIP’s current positioning of the ellipsoids, leading to a possible explanation for the modality gap.
6. We demonstrate how conformity can be used to quantify and rank image and text generators.
7. Leveraging this geometry, we develop *vertical SLERP* (*vSLERP*), which extends interpolation capabilities in spontaneous, training-free image generation.

2. Related Work

Contrastive representation learning is a powerful learning scheme, where models are trained to associate positive pairs (e.g., different views of the same image [6]) closely in the embedding space while pushing negative pairs (e.g., different images) apart. This simple yet effective approach has led to significant advances across a wide range of applications, i.e. image classification [6, 17], natural language processing [14, 30], 3D analysis [1, 55] and more.

The latent space induced by contrastive learning has been widely explored [2, 24, 51, 52], often conceptualized as a normalized hypersphere [35, 51]. Alignment and uniformity [51] are key properties of the *Normalized Temperature-scaled Cross-Entropy (NT-Xent)* loss [6]. Optimizing alignment and uniformity was shown to be crucial for preserving rich semantic structures in the latent space, leading to improvements in downstream performance across multiple domains [11].

With the rise of cross-modal contrastive models, such as CLIP [44], which align images and text in a shared embedding space, new challenges in latent space geometry have emerged. A notable issue is the modality gap [35], where embeddings from different modalities, such as images and text, are separated in the shared latent space. Moreover, the narrow cone effect was observed [35, 47], where features occupy only a limited portion of the angular space.

One of the main challenges in multimodal contrastive learning is of obtaining high-quality pairs. Web-scale datasets may include mismatched positive pairs [9, 12, 38, 50] or mislabeled negative pairs that are actually positive, referred to as *false negatives* [3, 33, 56]. Numerous approaches have emerged to address this challenge, such as by identifying and introducing hard negative examples [4, 8, 25, 46]. Our observations are that false negatives appear to play a significant role in forming the geometry of CLIP’s latent space.

3. Random vectors in high dimensions

3.1. Notations

We investigate CLIP space induced by ViT-B/32 encoders of $n = 512$ dimensions, $\mathcal{X} = R^n$. Let $\mathcal{X}_i \subset \mathcal{X}$ be the *image* subspace and $\mathcal{X}_t \subset \mathcal{X}$ be the *text* (captions) subspace. We will see that they are different and in fact linearly separable. Let $v \in \mathcal{X}$ be a vector in this space. We denote by $v_i \in \mathcal{X}_i$ vectors of images and by $v_t \in \mathcal{X}_t$ vectors of text. The symbol \mathbb{E} stands for the expected value. The respective modality mean of image and text are $m_i = \mathbb{E}_{v_i \in \mathcal{X}_i} [v_i]$ and $m_t = \mathbb{E}_{v_t \in \mathcal{X}_t} [v_t]$. Let \tilde{v} be the vector after subtraction of the respective modality mean. That is, for images, $\tilde{v}_i = v_i - m_i : v_i \in \mathcal{X}_i$ and for text $\tilde{v}_t = v_t - m_t : v_t \in \mathcal{X}_t$.

Our statistical analysis and many experimental results are based on MS-COCO [36] validation set, a common stan-

ard image-text dataset.

3.2. High dimensional geometry of random vectors

It is often challenging to obtain good intuition on the probability manifold and its geometry in high dimensions. We outline below some fundamental concepts.

3.2.1 Thin shell theory

There is an intensive research related to the thin shell phenomenon [23, 26, 31, 32, 43]. Definitions of *log concave distributions* and *isotropic random vectors* appear in the supplementary. Since isotropic random vectors have a unit second moment for any $x(k)$, $k = 1, ..n$, we get that the expected value of the squared Euclidean norm is

$$\mathbb{E}[\|x\|^2] = \mathbb{E}\left[\sum_{k=1}^n x(k)^2\right] = \sum_{k=1}^n \mathbb{E}[x(k)^2] = n. \quad (1)$$

As shown for example in [43], $\mathbb{E}[\|x\|^2] \approx \mathbb{E}^2[\|x\|]$, the expected norm of x can be approximated by

$$\mathbb{E}[\|x\|] \approx \sqrt{n}. \quad (2)$$

For isotropic log-concave distributions we have the *thin shell* property:

Theorem 3.1 (Thin shell). *Let the thin shell parameter be defined by*

$$\sigma_n^2 = \sup_x \mathbb{E}(\|x\| - \sqrt{n})^2,$$

where the supremum is over isotropic, log-concave random vectors in R^n . Then $\sigma_n \leq c(\log n)^\alpha$, where c is a universal constant.

Recent studies have shown this bound for $\alpha = 4$ [32], $\alpha = 2.23$ [23] and most recently for $\alpha = \frac{1}{2}$ [31]. See more details in the above papers and the references therein. Essentially, this means the mass of the distribution is concentrated around a shell of radius \sqrt{n} .

Let us farther examine this for the more general anisotropic case. Let $x = (x(1), \dots, x(n))$ be a vector of n random variables of different distributions (not iid), each of mean zero. Let the norm of x , which is a random variable, be defined by $\|x\| = \mu_{norm} + y$, where $\mu_{norm} := \mathbb{E}[\|x\|]$ and y is a random variable of zero mean. We examine the term $\mathbb{E}[\|x\|^2] = \text{tr}(\mathbb{C})$, where tr is the trace and \mathbb{C} is the covariance matrix of x :

$$\begin{aligned} \mathbb{E}[\|x\|^2] &= \mathbb{E}[(\mu_{norm} + y)^2] \\ &= \mathbb{E}[\mu_{norm}^2 + 2\mu_{norm}y + y^2] = \mu_{norm}^2 + \text{var}(y). \end{aligned} \quad (3)$$

Therefore, for $\mu_{norm}^2 \gg \text{var}(y)$ we can approximate

$$\mathbb{E}[\|x\|] = \mu_{norm} \approx \sqrt{\mathbb{E}[\|x\|^2]} = \sqrt{\text{tr}(\mathbb{C})}. \quad (4)$$

Here the squared expected Euclidean norm and the trace of the covariance matrix approximately coincide. We can thus view $\text{std}(x(k))$ as a rescale of the coordinate system in dimension k , with respect to a unit sphere.

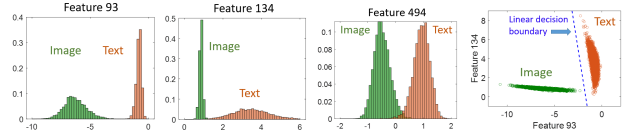


Figure 2. Normalized histograms of certain CLIP features. Image and text are clearly drawn from different statistics. On the right it is shown that even two features are sufficient to obtain full linear separability. The results of a linear SVM classifier are shown (blue dashed line, with 100% accuracy on MS-COCO).

4. Geometric Analysis

We begin by examining the statistics of image and text in the CLIP embedding space \mathcal{X} . This part is completely data-driven without any prior assumptions related to the training process. We focus on *the raw CLIP embedding*, which is the output of the encoder before L_2 normalization, i.e. before projection onto the unit hypersphere. This projection loses important information. It basically “flattens” the original geometry artificially, in a manner which is hard to analyze. More details and statistical data are provided in the Supp.

Let us first examine the known modality gap phenomenon [35] in the raw embedding. In Fig. 2, normalized histograms are shown for features 93, 134 and 494 of the CLIP latent vector. We get a bimodal distribution where image and text are clearly not drawn from the same distribution. For feature 93, for instance, the KL-divergence between the distributions is ≈ 301 (a value above 1 implies a considerable deviation between the distributions). It was previously shown in [11, 48] that image and text can be separated linearly. We find there are actually 9 features which serve as sort of “tags” for image and text. More formally, we can define the measure of separability of a feature ℓ by

$$\text{Sep}(\ell) = \frac{|m_i(\ell) - m_t(\ell)|}{\sqrt{\text{var}(v_i(\ell)) + \text{var}(v_t(\ell))}}. \quad (5)$$

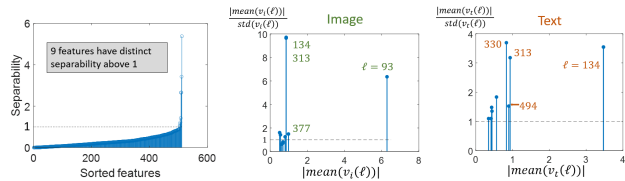


Figure 3. Separability of features (left) and 10 most significant features ℓ for image and text, with high absolute mean, compared to the feature’s standard deviation.

A plot of the features sorted by separability is shown in Fig. 3 (left). In Fig. 2 (right) it is shown that the modalities are linearly separable (with 100% accuracy) using only two such tag features (93 and 134), based on a linear SVM classifier (decision boundary shown in blue). We can thus state the following property (which holds exactly at least for MS-COCO):

Property 1: Image and text reside on separate sub-spaces, $\mathcal{X}_i \cap \mathcal{X}_t \approx \emptyset$.

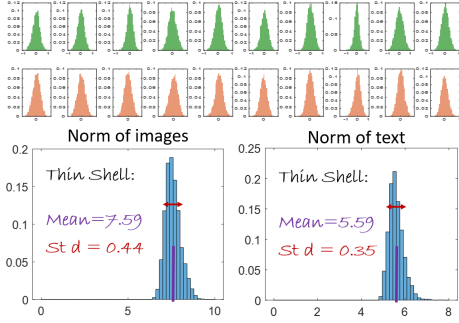


Figure 4. Illustration of statistics of image and text features after subtracting the mean for each modality. Top, histograms of 10 first features of image (first row) and text (second row). Bottom, histograms of $\|\tilde{v}\|$ of images and of text. Although each feature separately has most of the volume near zero, the distribution of $\|\tilde{v}\|$ has no volume below some threshold, indicating a thin shell phenomenon, typical for high dimensions.

In Fig. 4, we show some statistics of the features of \tilde{v}_i and \tilde{v}_t (where the mean is subtracted). The first 10 features in each vector are shown for both modalities. The distribution appears smooth, unimodal, with peak around zero. The norm $\|\tilde{v}\|$, however, is distributed within a small range (thin shell) such that there is no mass near zero.

We can further check the validity of Eq. (3), we examine images here. In the case of MS-COCO statistics we have: $\mu_{norm} = 7.5873$, $\text{var}(y) = 0.1914$, yielding $\mu_{norm}^2 = 57.5671 \gg \text{var}(y)$, where the approximation $\sqrt{\mathbb{E}[\|x\|^2]} = 7.6007$ is just with 0.18% relative error. We can therefore conclude:

Property 2: The mass of each modality is concentrated within a thin shell, with zero mass near the mean of the distribution.

Let us now investigate the geometry of each shell. We examine the variance of each feature ℓ . In a uniform hypersphere embedding we expect to have similar variance for all dimensions. We observe in Fig. 5 (left part) this is not the case, with a long tail distribution, where some features exhibit considerably larger variance, hence an ellipsoid structure:

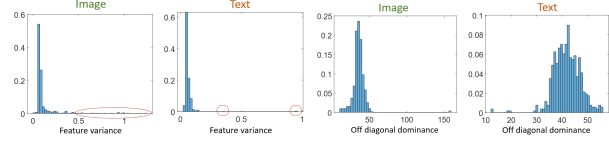


Figure 5. Normalized histograms of the variance of features (two left plots) indicates a long tail of high variance, hence an ellipsoid rather than an hypersphere. Off diagonal dominance, Eq. (6), implies certain strong feature correlations, or a tilted ellipsoid.

Property 3: The embedding of both text and image is of an ellipsoid shell.

We now examine inter-correlations between features. Let us define *off-diagonal dominance* of a row ℓ in the covariance matrix \mathbb{C} by

$$ODD(\ell) = \frac{\sum_{k \neq \ell} |\mathbb{C}_{\ell k}|}{\mathbb{C}_{\ell \ell}}. \quad (6)$$

Diagonally dominant matrices have $ODD(\ell) < 1, \forall \ell$ ensuring a non-singular matrix. We observe (see Fig. 5 two right plots) that the off diagonals are significant, implying non-negligible correlation between features, thus:

Property 4: The ellipsoids of both modalities are tilted.

Finally, we check the location of each ellipsoid, with respect to the origin. We recall $m_i, m_t \in R^n$ are the mean value vectors of image and text. Let $\sigma_i, \sigma_t \in R^n$ be the standard deviation vectors of image and text, respectively. We have $\frac{\|m_i\|}{\|\sigma_i\|} = 0.94$ and $\frac{\|m_t\|}{\|\sigma_t\|} = 1.03$. Viewing $\|\sigma\|$ as a mean vector magnitude of the ellipsoid shell, the means are significantly shifted from the origin, compared to the size of the ellipsoid. This is caused by a few features, with strong deviation from the origin (compared to the respective feature’s standard deviation), as shown in Fig. 3 (middle and right). Thus we can state:

Property 5: The ellipsoids are not centered near the origin.

A linear transformation can be applied to the embedding to transform the ellipsoid into a sphere. This process is called whitening [10, 28]. Analysis of whitened CLIP is in the supplementary, providing indications that multivariate normal distribution is a rather crud approximation.

5. Loss behavior on a double-ellipsoid

In this section, we validate that a shifted double-ellipsoid structure achieves optimality in terms of the CLIP contrastive learning loss.

For a batch containing M image-text pairs, we denote by $\bar{v}_i^j = \frac{v_i^j}{\|v_i^j\|}$ and $\bar{v}_t^j = \frac{v_t^j}{\|v_t^j\|}$ the normalized image and text features of the j -th pair in the batch respectively. The multi-modal learning loss used in CLIP is the *normalized temperature-scaled cross entropy loss* (NT-Xent), a variation of InfoNCE [42] loss:

$$\ell_{clip} := -\frac{1}{2} \mathbb{E}_{j,k \in M} \left[\log \frac{e^{\bar{v}_t^j \top \bar{v}_i^j / \tau}}{\sum_j e^{\bar{v}_t^j \top \bar{v}_i^k / \tau}} + \log \frac{e^{\bar{v}_t^k \top \bar{v}_i^j / \tau}}{\sum_j e^{\bar{v}_t^k \top \bar{v}_i^j / \tau}} \right]. \quad (7)$$

As observed by [51], the loss can be decomposed into two terms: (1) *Alignment*, which encourages high cosine similarity for positive pairs, and (2) *Uniformity*, which encourages low cosine similarity among negative samples.

$$\ell_{clip} := - \overbrace{\mathbb{E}_{j \in M} [\bar{v}_t^j \top \bar{v}_i^j / \tau]}^{\text{alignment}} + \overbrace{\mathbb{E}_{k \in M} \left[\frac{1}{2} \log \sum_{j=1}^M e^{\bar{v}_t^j \top \bar{v}_i^k / \tau} + \frac{1}{2} \log \sum_{j=1}^M e^{\bar{v}_t^k \top \bar{v}_i^j / \tau} \right]}^{\text{uniformity}}. \quad (8)$$

To empirically analyze the uniformity and alignment terms in Eq. (8) alongside the overall loss in Eq. (7), we use the MS-COCO validation set. Fig. 6 shows the overall loss (bottom) and its breakdown into uniformity and alignment losses (top). We treat the entire validation set (5k samples) as a single batch. The overall loss is further separated into correctly classified, misclassified, and combined cases; the union of the correct and misclassified is equivalent to both, and they are mutually exclusive.

In this experiment, we examine different values of the mean value of the image embedding. For simplicity, we apply linear interpolation and extrapolation of the mean relative to the origin, using a single scalar parameter α . This measure is conducted on a grid of α values from -1 to 1, with the loss calculated on image features as follows:

$$v_i^{j'} = v_i^j - \alpha \cdot m_i \quad \forall j \in M. \quad (9)$$

The values of v_t remain unchanged.

The results show that the loss for correctly classified samples decreases monotonically with the shift toward the origin (i.e. that for perfect alignment as assumed for example by [35], shifting to the origin would be preferable). Conversely, the loss for misclassified samples increases. The overall loss balances alignment and uniformity for both correctly and misclassified samples, reaching an optimal α near zero. This aligns with the current CLIP embedding, though some deviation is expected, as the MS-COCO validation set is only an approximation of the full training set.

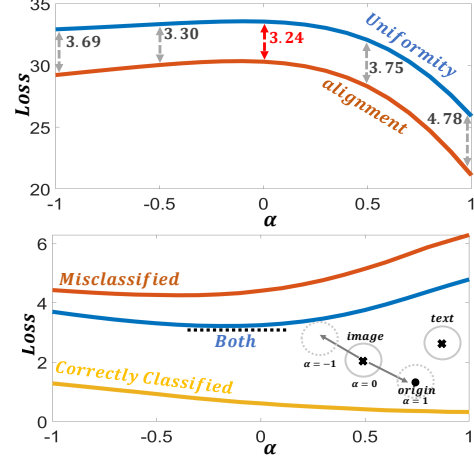


Figure 6. **Loss with respect to position of center of embedding.** The parameter α controls the center of embedding, see Eq. (9) ($\alpha = 0$ is the current non-origin-centered position of CLIP). (Top). For non-origin-centered position, the unified loss is optimally balancing between uniformity and alignment. (Bottom). The loss is ascending when only misclassified instances are examined, and descending for well-classified. The overall accuracy, contains both, well balanced at $\alpha \approx 0$.

For completeness, the supplementary material includes the same experiment with the text ellipsoid shifted instead of the image, showing consistent behavior. To conclude:

Property 6: CLIP’s contrastive loss is optimized for shifted ellipsoids, balancing alignment and uniformity for both correctly classified and misclassified instances.

6. False Negatives and Conformity

We show here how the geometric structure of the embedding, found in previous sections, is advantageous when false negatives exist. We then propose the notion of *conformity*, which appears to play a major role in forming the distribution of the latent space.

In contrastive learning, a well known problem is the phenomenon of false negatives. Essentially, concepts which are not dedicated pairs have similar meaning. Thus, they do not represent well negative examples and should not be embedded far apart. This problem appears for both single and multi-modality cases. There have been several suggestions to solve this problem by introducing new learning procedures or proposing alternative contrastive losses [4, 8].

In the case of CLIP, however, the training is performed with a contrastive loss which does not take into consideration directly the false negative problem. We claim that the issue is mitigated, to some extent, by a specialized embedding. In classification and segmentation, as uncertainty

grows, the network yields softer values, representing the lower membership probability to the class. In Fig. 7 (top) a typical segmentation score of semantic segmentation is shown, where the boundary of the sheep is blurred, due to reduced confidence. We refer to this as *semantic blur*. For a contrastive network, when false negatives are suspected we expect lower confidence and a more blurred response. In the case of a high dimensional sphere centered at the origin, blurring is not trivial. Small perturbations yield large disparities in cosine distance. We show below how a sphere not centered at the origin can mitigate this.

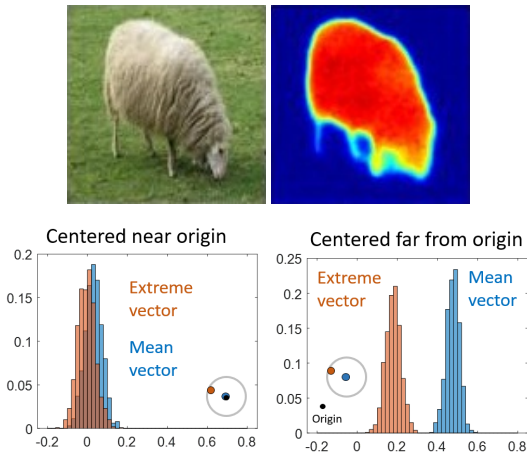


Figure 7. Top: blur of the segmentation score (right), typical in semantic segmentation, as the uncertainty of object-membership grows. Bottom: the similarity histograms of normally distributed samples are shown for the mean vector (blue) and a vector furthest from the mean (“extreme”, orange). The plots are done for a sphere centered near the origin (left) and for one with a center far from the origin (right). See full details of the experiment in the text. In the case of contrastive learning, blur can be achieved, as uncertainty grows, by having a sphere centered far from the origin. The desired blur can be controlled by positioning the embedded vector closer to the sphere center (blur) or farther from it (sharp).

Blur through a non-origin centered sphere. In Fig. 7 (bottom) we show an experiment that illustrates the difference between origin-centered and origin-non-centered spheres. We draw 1000 random vectors v^j of length 512, where each vector element is distributed independently according to normal (Gaussian) distribution with unit standard deviation. In the first experiment (Fig. 7 bottom left), the distribution is of mean zero. The empirical mean m is close to zero (but not exactly). In blue, a histogram of $\cos(m, v^j)$, $j = 1, \dots, 1000$ is shown. Next, we take the furthest vector from m , $v^{\text{far}} = \arg \min \cos(m, v^j)$, and show in orange the histogram of $\cos(v^{\text{far}}, v^j) : \forall j, v^j \neq v^{\text{far}}$. In Fig. 7 bottom right the sphere is centered at $(10, 5, 5, 0, 0, \dots)$. We perform the same trial. We observe the significant difference in the results of these two scenarios: for a sphere centered

near the origin, the distributions of the cosine similarity of the mean and a vector far from the mean (extreme vector) are similar. On the other hand, when the sphere is centered far from the origin, the similarity is much larger on average with respect to the mean vector. Thus, in cases of uncertainty, the network can embed such vectors near the mean vector, allowing *semantic blur*, that is - less contrast in the response. Our discussion above, which justifies non-zero mean, further leads to the following prediction:

Prediction 1: Common themes, which occur more frequently in the training set, are expected to be embedded in closer proximity to the mean vector.



Figure 8. **High and low conformity of natural images from MS-COCO [36].** Low-conformity images often depict unique, distinguishable individuals or objects, whereas high-conformity images capture common scenes that could be found anywhere.

6.1. Conformity

In order to validate our prediction, we first formalize the term *common themes*, by defining a new notion, termed *conformity*.

Definition 1 (Conformity). *Conformity of a vector v^j within a set S measures the expected value of the cosine similarity to this vector:*

$$C(v^j) = \mathbb{E}_{\substack{v^k \in S \\ j \neq k}} [\cos(v^j, v^k)], \quad (10)$$

where for a given finite set S , the empirical mean is taken.

To provide more intuition, we present examples of high and low conformity from MS-COCO in Fig. 8, as well as on ImageNet-a [21] and ImageNet-R [20] in the Supp. Following our prediction above, we propose a surrogate measure of conformity (which is much faster to compute). The estimation uses the following definition.

Definition 2 (Estimated conformity). *In contrastive learning embedding, for a given set of vectors S with mean $m = \mathbb{E}_{v \in S}[v]$, the estimated conformity of $v^j \in S$ is:*

$$\hat{C}(v^j) = a \cdot \cos(m, v^j) + b, \quad (11)$$

where a and b are scalars determined by the specific embedding.

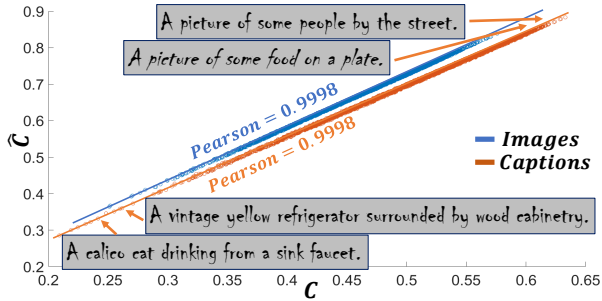


Figure 9. **Conformity.** Estimated conformity \hat{C} , Eq. (11), against conformity C , Eq. (10), on MS-COCO [36]. The correlation is almost perfect. We can thus use the proposed estimated conformity reliably to quantify how common a sample is. Employing \hat{C} is much faster, using a single mean vector m , without the need to store an entire set of representative image-text pairs. We also show a few caption examples of high and low conformity, with the same number of words (8). More exotic captions have lower conformity.

In Fig. 9, C versus \hat{C} are plotted for the entire MS-COCO set, for both image and text embeddings. A close to perfect correlation is obtained, with Pearson correlation of 0.9998 for both image and text where $a = 1.411$, $b = -0.008$ for text and $a = 1.461$, $b = -0.002$ for images.

6.2. Modality gap assists in distribution matching

We now aim to provide a reason that can justify the presence of the well known *modality gap* [35]. Our rationale for that phenomenon is as follows.

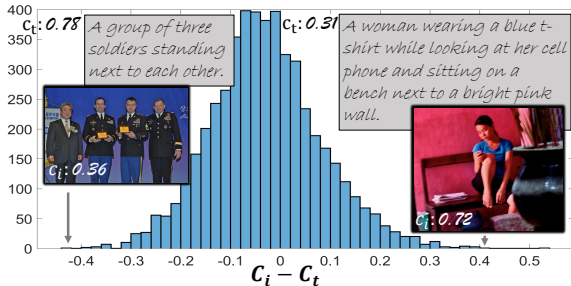


Figure 10. **Conformity Differences.** The conformity distributions of text and image modalities differ, as a common image may be described by a unique caption, and vice versa.

The same incentive of having a mean not centered at the origin applies for both image and text modalities. However, in a single image-pair instance the uncertainty for each modality may differ (see Fig. 10). The same arguments as before promote uncertain instances to be near the mean and certain ones to be far from it. If both image and text of a pair are embedded at the same location - we may get contradicting requirements. Having separate embeddings for text and image allows to control the uncertainty of each instance for

each modality. More generally, we would like to match the distribution of the conformity of both modalities. In Fig. 11 we show the KL-divergence of the conformity distribution as a function of α , a parameter controlling the distance of the mean from the origin, as in Eq. (9), see illustration in Fig. 6. We show that the best distribution match is near $\alpha = 0$, that is, in the current embedding of CLIP.

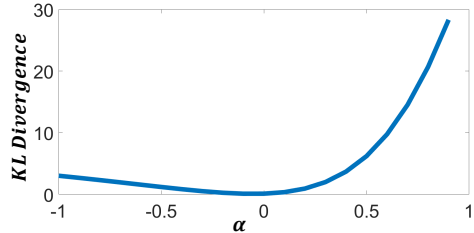


Figure 11. **Matching the distribution of conformity for image and text by introducing a modality gap.** The parameter α controls the shift from the origin for images (as in Fig. 6). Both image and text conformity distributions are aligned when $\alpha \approx 0$, i.e. without any shift from the trained setting. $KL_{\alpha=0} \approx 0.14$ yields a good distribution matching.

7. Applications

7.1. Conformity as a measure of expressiveness

We propose to use (estimated) conformity as a metric to assess the richness of generative methods. Specifically, we measure the conformity of images generated from MS-COCO captions by unCLIP [45] and Glide [41], visualizing the results in Fig. 13. Glide-generated images exhibit high conformity, indicating less detail and diversity, whereas unCLIP images are more varied and detailed. However, both models fall short of matching the diversity found in real images.

Similarly, we evaluate captioning methods by measuring conformity in captions generated using ClipCap [40] and Caption Reward [7]. ClipCap tends to produce common and trivial captions, while Caption Reward generates captions with diversity surpassing even human annotations.

7.2. Unguided, training-free semantic generation

The unCLIP framework [45] introduces an image interpolation technique using spherical linear interpolation (SLERP) to transform a source image into a target image gradually. While this method produces visually appealing results, it often fails to preserve the same instance throughout interpolation, instead generating random instances.

In Fig. 12, we show images generated by an extension of SLERP, which we term as *vertical SLERP* (*vSLERP*), defined as:

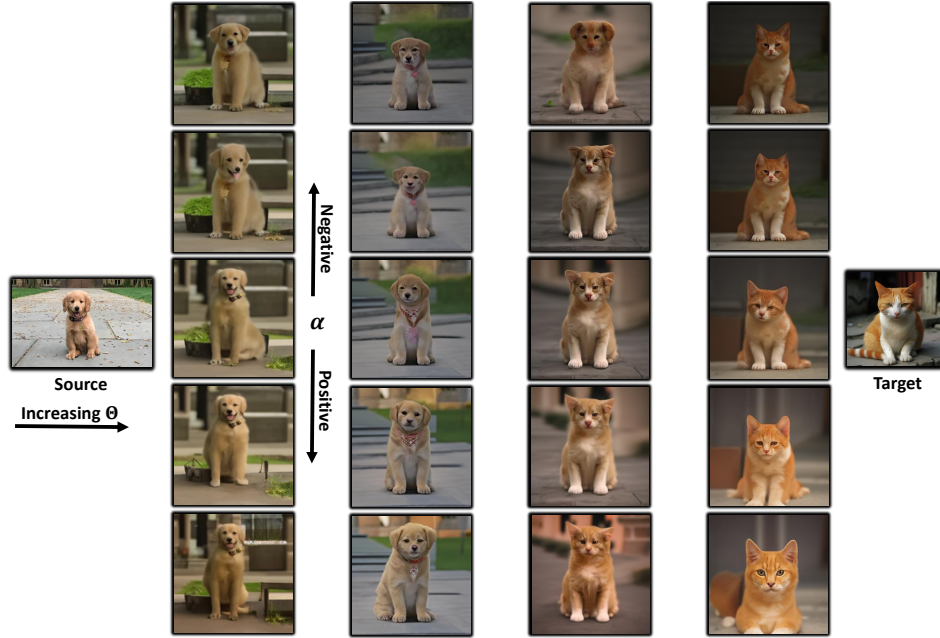


Figure 12. **Vertical SLERP (vSLERP) - Optimization-free, spontaneous semantic editing.** Images interpolated with vSLERP preserve the same object with slight pose variations, while roughly maintaining backgrounds. The interpolation magnitude is controlled by α .

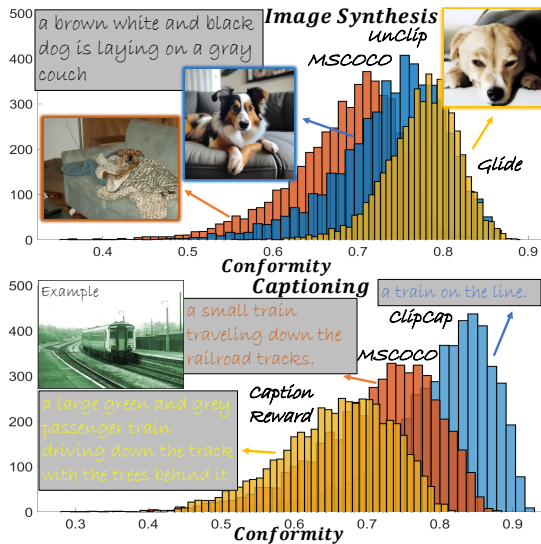


Figure 13. **Conformity analysis of Captioning and Image Synthesis.** *Image Synthesis (top):* Glide [41] tends to generate more common images, often struggling with fine-grained details, whereas unCLIP [45] generates images with more delicate details, aligning more closely with the distribution of natural images. Though there is still room for improvement. *Captioning (bottom):* ClipCap [40] generates captions with higher conformity (i.e., more common descriptions) compared to human-annotated captions. In contrast, Caption Reward [7] produces captions with lower conformity, even surpassing human annotations in terms of uniqueness.

$$vSLERP(v^j, v^k, \theta_0, \alpha) = SLERP(v^j - \alpha m, v^k - \alpha m, \theta_0) + \alpha m \quad (12)$$

For brevity, m_i and v_i are referred to as m and v . With a fixed $\Theta = \Theta_0$, adjusting α allows controlled manipulation of the same instance (values in the range $-2 \leq \alpha \leq 2$ tend to produce visually appealing images). This approach parallels real-image editing techniques; however, unlike methods relying on text inversion [13, 16, 39] or test-time optimization [27], which are computationally heavy, vSLERP requires no training or optimization, thus, highly efficient.

8. Discussion and Conclusion

This paper analyzes the raw CLIP embeddings before projection onto a unit hypersphere, revealing that each modality's distribution forms a distinct, shifted ellipsoid. These ellipsoids differ in properties such as their center of mass and radii and are disjoint, hence the modality gap phenomenon [35]. Upon projection onto a unit hypersphere, they occupy only a limited angular space, which appears as a narrow cone effect [35, 47]. We introduce the concept of *conformity*, a measure of similarity with the entire set, to gain further insights into the double-ellipsoid geometry. We observe that each modality has a unique conformity distribution, with optimal matching achieved when the ellipsoids are positioned away from the center. Using this framework, we evaluate the diversity of captioning and image synthesis methods and propose a training-free interpolation tech-

nique, *vertical SLERP* (vSLERP), for specific object interpolation.

References

- [1] Mohamed Afham, Isuru Dissanayake, Dinithi Dissanayake, Amaya Dharmasiri, Kanchana Thilakarathna, and Ranga Rodrigo. Crosspoint: Self-supervised cross-modal contrastive learning for 3d point cloud understanding. In *Proceedings of the IEEE/CVF Conference on Computer Vision and Pattern Recognition*, pages 9902–9912, 2022. 2
- [2] Sanjeev Arora, Hrishikesh Khandeparkar, Mikhail Khodak, Orestis Plevrakis, and Nikunj Saunshi. A theoretical analysis of contrastive unsupervised representation learning. *arXiv preprint arXiv:1902.09229*, 2019. 2
- [3] Jaeseok Byun, Taebaek Hwang, Jianlong Fu, and Taesup Moon. Grit-vlp: Grouped mini-batch sampling for efficient vision and language pre-training. In *European Conference on Computer Vision*, pages 395–412. Springer, 2022. 2
- [4] Jaeseok Byun, Dohoon Kim, and Taesup Moon. Mafa: Managing false negatives for vision-language pre-training. In *Proceedings of the IEEE/CVF Conference on Computer Vision and Pattern Recognition*, pages 27314–27324, 2024. 2, 5
- [5] Runnan Chen, Youquan Liu, Lingdong Kong, Xinge Zhu, Yuexin Ma, Yikang Li, Yuenan Hou, Yu Qiao, and Wengping Wang. Clip2scene: Towards label-efficient 3d scene understanding by clip. In *Proceedings of the IEEE/CVF Conference on Computer Vision and Pattern Recognition*, pages 7020–7030, 2023. 1
- [6] Ting Chen, Simon Kornblith, Mohammad Norouzi, and Geoffrey Hinton. A simple framework for contrastive learning of visual representations. In *International conference on machine learning*, pages 1597–1607. PMLR, 2020. 2
- [7] Jaemin Cho, Seunghyun Yoon, Ajinkya Kale, Franck Dernoncourt, Trung Bui, and Mohit Bansal. Fine-grained image captioning with clip reward. *arXiv preprint arXiv:2205.13115*, 2022. 1, 7, 8
- [8] Ching-Yao Chuang, Joshua Robinson, Yen-Chen Lin, Antonio Torralba, and Stefanie Jegelka. Debaised contrastive learning. *Advances in neural information processing systems*, 33:8765–8775, 2020. 2, 5
- [9] Sanghyuk Chun, Wonjae Kim, Song Park, Minsuk Chang, and Seong Joon Oh. Eccv caption: Correcting false negatives by collecting machine-and-human-verified image-caption associations for ms-coco. In *European Conference on Computer Vision*, pages 1–19. Springer, 2022. 2
- [10] Yonina C. Eldar and Alan V. Oppenheim. Mmse whitening and subspace whitening. *IEEE Transactions on Information Theory*, 49(7):1846–1851, 2003. 4
- [11] Abrar Fahim, Alex Murphy, and Alona Fyshe. Its not a modality gap: Characterizing and addressing the contrastive gap. *arXiv preprint arXiv:2405.18570*, 2024. 1, 2, 3
- [12] Samir Yitzhak Gadre, Gabriel Ilharco, Alex Fang, Jonathan Hayase, Georgios Smyrnis, Thao Nguyen, Ryan Marten, Mitchell Wortsman, Dhruva Ghosh, Jieyu Zhang, et al. Datacomp: In search of the next generation of multimodal datasets. *Advances in Neural Information Processing Systems*, 36, 2024. 2
- [13] Rinon Gal, Yuval Alaluf, Yuval Atzmon, Or Patashnik, Amit H Bermano, Gal Chechik, and Daniel Cohen-Or. An image is worth one word: Personalizing text-to-image generation using textual inversion. *arXiv preprint arXiv:2208.01618*, 2022. 8
- [14] Tianyu Gao, Xingcheng Yao, and Danqi Chen. Simcse: Simple contrastive learning of sentence embeddings. *arXiv preprint arXiv:2104.08821*, 2021. 2
- [15] Andrey Guzhov, Federico Raue, Jörn Hees, and Andreas Dengel. Audioclip: Extending clip to image, text and audio. In *ICASSP 2022-2022 IEEE International Conference on Acoustics, Speech and Signal Processing (ICASSP)*, pages 976–980. IEEE, 2022. 1
- [16] Ligong Han, Song Wen, Qi Chen, Zhixing Zhang, Kunpeng Song, Mengwei Ren, Ruijiang Gao, Anastasis Stathopoulos, Xiaoxiao He, Yuxiao Chen, et al. Proxedit: Improving tuning-free real image editing with proximal guidance. In *Proceedings of the IEEE/CVF Winter Conference on Applications of Computer Vision*, pages 4291–4301, 2024. 8
- [17] Kaiming He, Haoqi Fan, Yuxin Wu, Saining Xie, and Ross Girshick. Momentum contrast for unsupervised visual representation learning. In *Proceedings of the IEEE/CVF conference on computer vision and pattern recognition*, pages 9729–9738, 2020. 2
- [18] Sunan He, Taian Guo, Tao Dai, Ruizhi Qiao, Xiujun Shu, Bo Ren, and Shu-Tao Xia. Open-vocabulary multi-label classification via multi-modal knowledge transfer. In *Proceedings of the AAAI Conference on Artificial Intelligence*, volume 37, pages 808–816, 2023. 1
- [19] Deepti Hegde, Jeya Maria Jose Valanarasu, and Vishal Patel. Clip goes 3d: Leveraging prompt tuning for language grounded 3d recognition. In *Proceedings of the IEEE/CVF International Conference on Computer Vision*, pages 2028–2038, 2023. 1
- [20] Dan Hendrycks, Steven Basart, Norman Mu, Saurav Kadavath, Frank Wang, Evan Dorundo, Rahul Desai, Tyler Zhu, Samyak Parajuli, Mike Guo, et al. The many faces of robustness: A critical analysis of out-of-distribution generalization. In *Proceedings of the IEEE/CVF international conference on computer vision*, pages 8340–8349, 2021. 6
- [21] Dan Hendrycks, Kevin Zhao, Steven Basart, Jacob Steinhardt, and Dawn Song. Natural adversarial examples. In *Proceedings of the IEEE/CVF conference on computer vision and pattern recognition*, pages 15262–15271, 2021. 6
- [22] Tri Huynh, Simon Kornblith, Matthew R Walter, Michael Maire, and Maryam Khademi. Boosting contrastive self-supervised learning with false negative cancellation. In *Proceedings of the IEEE/CVF winter conference on applications of computer vision*, pages 2785–2795, 2022. 2
- [23] Arun Jambulapati, Yin Tat Lee, and Santosh S Vempala. A slightly improved bound for the kls constant. *arXiv preprint arXiv:2208.11644*, 2022. 3
- [24] Wenlong Ji, Zhun Deng, Ryumei Nakada, James Zou, and Linjun Zhang. The power of contrast for feature learning: A theoretical analysis. *Journal of Machine Learning Research*, 24(330):1–78, 2023. 2

- [25] Yannis Kalantidis, Mert Bulent Sariyildiz, Noe Pion, Philippe Weinzaepfel, and Diane Larlus. Hard negative mixing for contrastive learning. *Advances in neural information processing systems*, 33:21798–21809, 2020. [2](#)
- [26] Ravi Kannan, László Lovász, and Miklós Simonovits. Isoperimetric problems for convex bodies and a localization lemma. *Discrete & Computational Geometry*, 13:541–559, 1995. [3](#)
- [27] Bahjat Kawar, Shiran Zada, Oran Lang, Omer Tov, Huiwen Chang, Tali Dekel, Inbar Mosseri, and Michal Irani. Imagic: Text-based real image editing with diffusion models. In *Proceedings of the IEEE/CVF Conference on Computer Vision and Pattern Recognition*, pages 6007–6017, 2023. [1](#), [8](#)
- [28] Agnan Kessy, Alex Lewin, and Korbinian Strimmer. Optimal whitening and decorrelation. *The American Statistician*, 72(4):309–314, 2018. [4](#)
- [29] Gwanghyun Kim, Taesung Kwon, and Jong Chul Ye. Diffusionclip: Text-guided diffusion models for robust image manipulation. In *Proceedings of the IEEE/CVF conference on computer vision and pattern recognition*, pages 2426–2435, 2022. [1](#)
- [30] Taek Kim, Kang Min Yoo, and Sang-goo Lee. Self-guided contrastive learning for bert sentence representations. *arXiv preprint arXiv:2106.07345*, 2021. [2](#)
- [31] Bo’az Klartag. Logarithmic bounds for isoperimetry and slices of convex sets. *Ars Inveniendi Analytica*, 4, 2023. [1](#), [3](#)
- [32] Bo’az Klartag and Joseph Lehec. Bourgain’s slicing problem and kls isoperimetry up to polylog. *Geometric and functional analysis*, 32(5):1134–1159, 2022. [1](#), [3](#)
- [33] Junnan Li, Dongxu Li, Caiming Xiong, and Steven Hoi. Blip: Bootstrapping language-image pre-training for unified vision-language understanding and generation. In *International conference on machine learning*, pages 12888–12900. PMLR, 2022. [2](#)
- [34] Feng Liang, Bichen Wu, Xiaoliang Dai, Kunpeng Li, Yanan Zhao, Hang Zhang, Peizhao Zhang, Peter Vajda, and Diana Marculescu. Open-vocabulary semantic segmentation with mask-adapted clip. In *Proceedings of the IEEE/CVF Conference on Computer Vision and Pattern Recognition*, pages 7061–7070, 2023. [1](#)
- [35] Victor Weixin Liang, Yuhui Zhang, Yongchan Kwon, Serena Yeung, and James Y Zou. Mind the gap: Understanding the modality gap in multi-modal contrastive representation learning. *Advances in Neural Information Processing Systems*, 35:17612–17625, 2022. [1](#), [2](#), [3](#), [5](#), [7](#), [8](#)
- [36] Tsung-Yi Lin, Michael Maire, Serge Belongie, James Hays, Pietro Perona, Deva Ramanan, Piotr Dollár, and C Lawrence Zitnick. Microsoft coco: Common objects in context. In *Computer Vision—ECCV 2014: 13th European Conference, Zurich, Switzerland, September 6–12, 2014, Proceedings, Part V 13*, pages 740–755. Springer, 2014. [1](#), [2](#), [6](#), [7](#)
- [37] Huaishao Luo, Lei Ji, Ming Zhong, Yang Chen, Wen Lei, Nan Duan, and Tianrui Li. Clip4clip: An empirical study of clip for end to end video clip retrieval and captioning. *Neurocomputing*, 508:293–304, 2022. [1](#)
- [38] Pratyush Maini, Sachin Goyal, Zachary C Lipton, J Zico Kolter, and Aditi Raghunathan. T-mars: Improving visual representations by circumventing text feature learning. *arXiv preprint arXiv:2307.03132*, 2023. [2](#)
- [39] Ron Mokady, Amir Hertz, Kfir Aberman, Yael Pritch, and Daniel Cohen-Or. Null-text inversion for editing real images using guided diffusion models. In *Proceedings of the IEEE/CVF Conference on Computer Vision and Pattern Recognition*, pages 6038–6047, 2023. [8](#)
- [40] Ron Mokady, Amir Hertz, and Amit H Bermano. Clipcap: Clip prefix for image captioning. *arXiv preprint arXiv:2111.09734*, 2021. [1](#), [7](#), [8](#)
- [41] Alex Nichol, Prafulla Dhariwal, Aditya Ramesh, Pranav Shyam, Pamela Mishkin, Bob McGrew, Ilya Sutskever, and Mark Chen. Glide: Towards photorealistic image generation and editing with text-guided diffusion models. *arXiv preprint arXiv:2112.10741*, 2021. [1](#), [7](#), [8](#)
- [42] Aaron van den Oord, Yazhe Li, and Oriol Vinyals. Representation learning with contrastive predictive coding. *arXiv preprint arXiv:1807.03748*, 2018. [5](#)
- [43] Grigoris Paouris. Concentration of mass on convex bodies. *Geometric & Functional Analysis GAFA*, 16(5):1021–1049, 2006. [3](#)
- [44] Alec Radford, Jong Wook Kim, Chris Hallacy, Aditya Ramesh, Gabriel Goh, Sandhini Agarwal, Girish Sastry, Amanda Askell, Pamela Mishkin, Jack Clark, et al. Learning transferable visual models from natural language supervision. In *International conference on machine learning*, pages 8748–8763. PMLR, 2021. [1](#), [2](#)
- [45] Aditya Ramesh, Prafulla Dhariwal, Alex Nichol, Casey Chu, and Mark Chen. Hierarchical text-conditional image generation with clip latents. *arXiv preprint arXiv:2204.06125*, 1(2):3, 2022. [1](#), [7](#), [8](#)
- [46] Joshua Robinson, Ching-Yao Chuang, Suvrit Sra, and Stefanie Jegelka. Contrastive learning with hard negative samples. *arXiv preprint arXiv:2010.04592*, 2020. [2](#)
- [47] Simon Schrodi, David T Hoffmann, Max Argus, Volker Fischer, and Thomas Brox. Two effects, one trigger: On the modality gap, object bias, and information imbalance in contrastive vision-language representation learning. *arXiv preprint arXiv:2404.07983*, 2024. [1](#), [2](#), [8](#)
- [48] Peiyang Shi, Michael C Welle, Márten Björkman, and Danica Kragic. Towards understanding the modality gap in clip. In *ICLR 2023 Workshop on Multimodal Representation Learning: Perks and Pitfalls*, 2023. [3](#)
- [49] Mingkang Tang, Zhanyu Wang, Zhenhua Liu, Fengyun Rao, Dian Li, and Xiu Li. Clip4caption: Clip for video caption. In *Proceedings of the 29th ACM International Conference on Multimedia*, pages 4858–4862, 2021. [1](#)
- [50] Alex Jinpeng Wang, Kevin Qinghong Lin, David Junhao Zhang, Stan Weixian Lei, and Mike Zheng Shou. Too large; data reduction for vision-language pre-training. In *Proceedings of the IEEE/CVF International Conference on Computer Vision*, pages 3147–3157, 2023. [2](#)
- [51] Tongzhou Wang and Phillip Isola. Understanding contrastive representation learning through alignment and uniformity on the hypersphere. In *International conference on machine learning*, pages 9929–9939. PMLR, 2020. [2](#), [5](#)

- [52] Yifei Wang, Qi Zhang, Yisen Wang, Jiansheng Yang, and Zhouchen Lin. Chaos is a ladder: A new theoretical understanding of contrastive learning via augmentation overlap. *arXiv preprint arXiv:2203.13457*, 2022. [2](#)
- [53] Ho-Hsiang Wu, Prem Seetharaman, Kundan Kumar, and Juan Pablo Bello. Wav2clip: Learning robust audio representations from clip. In *ICASSP 2022-2022 IEEE International Conference on Acoustics, Speech and Signal Processing (ICASSP)*, pages 4563–4567. IEEE, 2022. [1](#)
- [54] Xiaoshi Wu, Feng Zhu, Rui Zhao, and Hongsheng Li. Cora: Adapting clip for open-vocabulary detection with region prompting and anchor pre-matching. In *Proceedings of the IEEE/CVF conference on computer vision and pattern recognition*, pages 7031–7040, 2023. [1](#)
- [55] Saining Xie, Jiatao Gu, Demi Guo, Charles R Qi, Leonidas Guibas, and Or Litany. Pointcontrast: Unsupervised pre-training for 3d point cloud understanding. In *Computer Vision–ECCV 2020: 16th European Conference, Glasgow, UK, August 23–28, 2020, Proceedings, Part III 16*, pages 574–591. Springer, 2020. [2](#)
- [56] Jinyu Yang, Jiali Duan, Son Tran, Yi Xu, Sampath Chanda, Liqun Chen, Belinda Zeng, Trishul Chilimbi, and Junzhou Huang. Vision-language pre-training with triple contrastive learning. In *Proceedings of the IEEE/CVF Conference on Computer Vision and Pattern Recognition*, pages 15671–15680, 2022. [2](#)
- [57] Qihang Yu, Ju He, Xueqing Deng, Xiaohui Shen, and Liang-Chieh Chen. Convolutions die hard: Open-vocabulary segmentation with single frozen convolutional clip. *Advances in Neural Information Processing Systems*, 36, 2024. [1](#)
- [58] Renrui Zhang, Ziyu Guo, Wei Zhang, Kunchang Li, Xupeng Miao, Bin Cui, Yu Qiao, Peng Gao, and Hongsheng Li. Pointclip: Point cloud understanding by clip. In *Proceedings of the IEEE/CVF conference on computer vision and pattern recognition*, pages 8552–8562, 2022. [1](#)

The Double-Ellipsoid Geometry of CLIP

Supplementary Materials

arXiv:2411.14517v1 [cs.CV] 21 Nov 2024

1. Enlarged Visualizations

In Fig. 2 and Fig. 3, we provide the same visualizations as in the main paper, but enlarged, to enhance visibility. **CLIP of higher dimension.** We also show some results for CLIP with ViT-L/14 encoders, $n = 768$. In Fig. 4 we show the distinct different statistics of image and text, mostly appearing in several pronounced features. Here as well, linear separation (100% classification accuracy) can be reached with only two features. In Fig. 5 we show that the embedding can also be modeled as two separate thin shell ellipsoids for image and text.

2. Statistical Analysis

We provide here the definitions of log concave distributions and isotropic random vectors, notions which are used in Section 4 of the main paper.

Definition 1 (Log concave distribution). *A log concave distribution in R^n has a density p which admits, $\forall x, y \in R^n, \lambda \in [0, 1]$,*

$$p(\lambda x + (1 - \lambda)y) \geq p(x)^\lambda p(y)^{1-\lambda}.$$

The above definition is equivalent to stating that the logarithm of the density function is concave $\log p(\lambda x + (1 - \lambda)y) \geq \lambda \log p(x) + (1 - \lambda) \log p(y)$. Many well-known distributions admit this property, such as normal and multivariate normal distributions, exponential, Laplace, chi, Dirichlet, gamma and more.

Definition 2 (Isotropic random vector). *A random vector $x \in R^n$ is isotropic if $\mathbb{E}[x] = 0$ and $\Sigma = I$, where Σ is the covariance matrix of x and I is the identity matrix.*

We give below additional analysis related to applying a linear transformation that turns each ellipsoid into a sphere. This process is termed sphering or whitening. For lack of space, this part did not get into the main paper. However, we believe this analysis is of sufficient merit to be presented here.

2.1. Whitened CLIP

The above theory suggests we can expect the thin shell phenomenon. However, although the feature histograms ap-

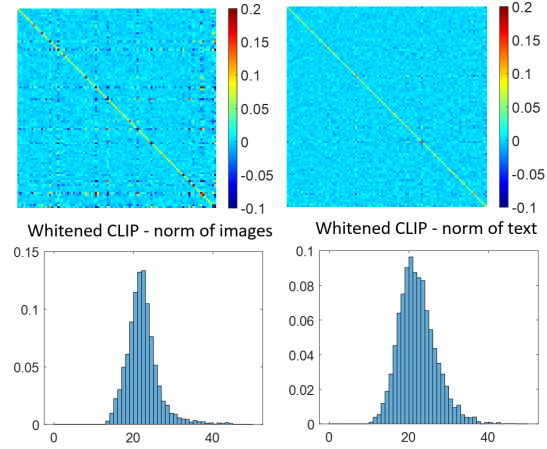


Figure 1. Top - covariance matrices of image and of text (first 100 features of each modality are shown). Both distributions are not isotropic. Bottom - histogram of norm of whitened CLIP, $\|y_i\|$, $\|y_t\|$. Here the spread of the norms is wider than the original embedding and not admitting a chi distribution. See mean and standard-deviation estimates following Claim 1.

pear to be drawn from log-concave distributions, both image and text CLIP embeddings certainly do not admit the isotropic property (see Fig. 1). To obtain isotropic behavior one can apply a whitening transform.

Definition 3 (Whitening transform). *Let x be a random vector in R^n with nonsingular covariance matrix Σ and mean zero. Let W be a whitening matrix satisfying the condition $W^T W = \Sigma^{-1}$. The whitening transform is defined by $y = Wx$. The random vector y is isotropic.*

One can choose $W = \Sigma^{-1/2}$, where any unitary matrix can be applied to W , maintaining the whitening property. We now would like to model the norm distribution of whitened CLIP.

Claim 1 (Thin shell of whitened CLIP). *Let $y_i = W_i(v - m_i)$, $v \in \mathcal{X}_i$, be a whitening transform of CLIP images and $y_t = W_t(v - m_t)$, $v \in \mathcal{X}_t$, be a whitening transform of CLIP text. The distribution of the norm admits the thin shell property. Moreover, the norm statistics of $y \in \{y_i, y_t\}$ can*

be well modeled by

$$m(y) := \mathbb{E}[\|y\|] \approx \sqrt{n} = \hat{m}(y), \quad (1)$$

$$s(y) := \text{std}(\|y\|) = \sqrt{n - m^2(y)} = \hat{s}(y). \quad (2)$$

The above claim is validated empirically, assuming MSCOCO represents well image and text statistics. In Fig. 1 (bottom) we show the norm distribution of $\|y_i\|$ and $\|y_t\|$. Let us first show the approximation of Eq. (1). For images $\mathbb{E}[\|y_i\|] = 22.261$ and for text $\mathbb{E}[\|y_t\|] = 22.144$, whereas $\sqrt{n} = 22.627$ (relative errors of 1.6% and 2.1%, respectively). The expression in Eq. (2) is based on the identity $\text{var}(x) = \mathbb{E}[x^2] - \mathbb{E}[x]^2$ and using Eq. (1) in the main paper. Naturally, as the approximation of Eq. (1) is better ($m(y) \rightarrow \sqrt{n}$), the standard deviation is lower.

We now would like to examine whether CLIP can be well approximated by a multivariate normal distribution. In that case, any linear combination of its n components has a univariate normal distribution. Specifically for isotropic random vectors, such as whitened CLIP, we should have normal distribution with zero mean and unit standard deviation. The norm then follows the chi distribution. Let us recall this for completeness. Let $z = \sqrt{\sum_{j=1}^n u_j^2}$, where u_j is a normally distributed random variable with zero mean and unit standard deviation. Then z follows the chi distribution with $\mathbb{E}[z] = \sqrt{2} \frac{\Gamma(n/2 + 1/2)}{\Gamma(n/2)}$, where Γ is the gamma function and $\text{std}(z) = \sqrt{n - \mathbb{E}[z]^2}$. As n increases we get $\mathbb{E}[z] \rightarrow \sqrt{n}$ and the rate of convergence is such that $\text{std}(z) \rightarrow \frac{1}{2}$. For $n = 512$ we reach very closely these values. Our experimental data shows that the standard deviations for image and text are $\text{std}(\|y_i\|) = 4.044$ and $\text{std}(\|y_t\|) = 4.641$, which are both much larger than $\frac{1}{2}$. Thus we cannot assume chi distribution of the norms and hence normal distribution for the whitened embeddings y_i, y_t . Our whitening process does not produce perfect results, but Eq. (2) holds quite accurately where the right-hand-side of Eq. (2) yields $\hat{s}(y_i) = 4.056$ and $\hat{s}(y_t) = 4.646$ (relative errors of 0.3% and 0.1%, respectively).

To conclude, whitened CLIP admits thin shell properties, however the shell is not that thin, and certainly not as thin as chi distribution (the shell is 8 to 9 times wider for $n = 512$). Thus, whitened CLIP of both image and text can be well estimated by some unknown log-concave distribution (for which normal distribution is a crude approximation). The original CLIP embeddings of both image and text can be approximated as multivariate log-concave distributions, exhibiting thin shells.

3. Additional Experiments and Visualizations

3.1. Conformity

High- and Low-Conformity Images. We provide additional visualizations of high- and low-conformity images

across various datasets. Figure 6 illustrates examples of sketches from ImageNet-R, while Figure 7 showcases examples from ImageNet-A. Both datasets contain out-of-distribution examples: ImageNet-A emphasizes natural adversarial images, while ImageNet-R features renditions of objects, such as origami or sketches.

From these visualizations, we observe that high-conformity images tend to contain less information. Sketches are simpler, and natural images often feature large uniform backgrounds or repetitive structures. In contrast, low-conformity images frequently include substantial text, while natural images exhibit collages of objects with unique or diverse colors.

3.2. Reaffirming Loss and Conformity Matching Experiments

We revisit the loss experiment presented in Fig. 6 of the main paper and the conformity matching experiment shown in Fig. 11. To further validate our findings, we conduct these experiments under two alternative settings.

First, we shift the text ellipsoid instead of the image ellipsoid, applying the following transformation:

$$v_t^{j'} = v_t^j - \alpha \cdot m_t \quad \forall j \in M, \quad (3)$$

where the values of v_i remain unchanged. The results of this experiment are presented in Fig. 8.

In the second setting, we align both the image and text ellipsoids at the origin by applying the following transformations:

$$v_t^{j'} = v_t^j - \alpha \cdot m_t, \quad v_i^{j'} = v_i^j - \alpha \cdot m_i \quad \forall j \in M. \quad (4)$$

Here, for $\alpha = 0$, the ellipsoids remain in their optimal positions after training, while for $\alpha = 1$, both ellipsoids are shifted to the origin as in Fig. 9.

Both experiments reaffirm that the current positioning of the ellipsoids yields optimal results in terms of loss and conformity matching. These findings further support our claims across different alignment scenarios.

3.3. vSLERP

Here, we provide additional examples of vSLERP, shown in Fig. 10 and Fig. 11. As discussed in the main paper, the standard SLERP process typically generates interpolated images representing different objects or individuals. In contrast, our proposed vSLERP method produces diverse variations of the same object.

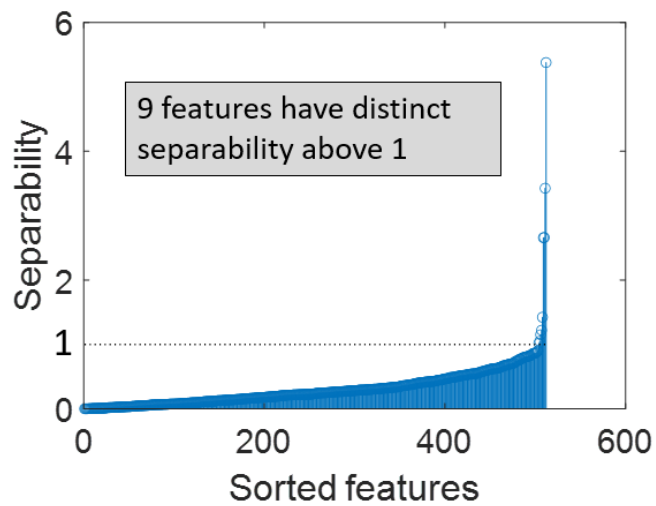
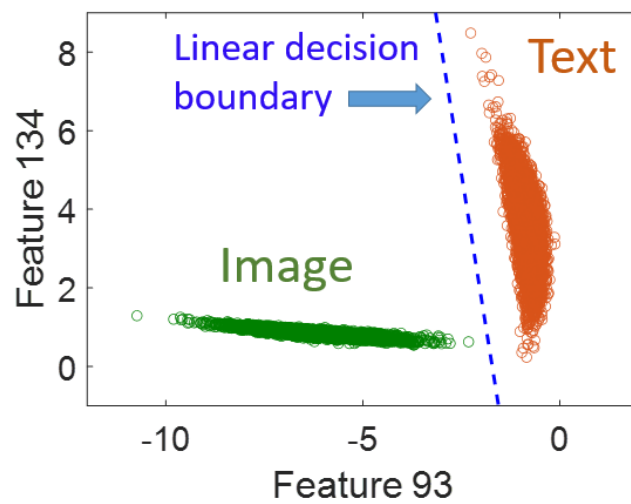
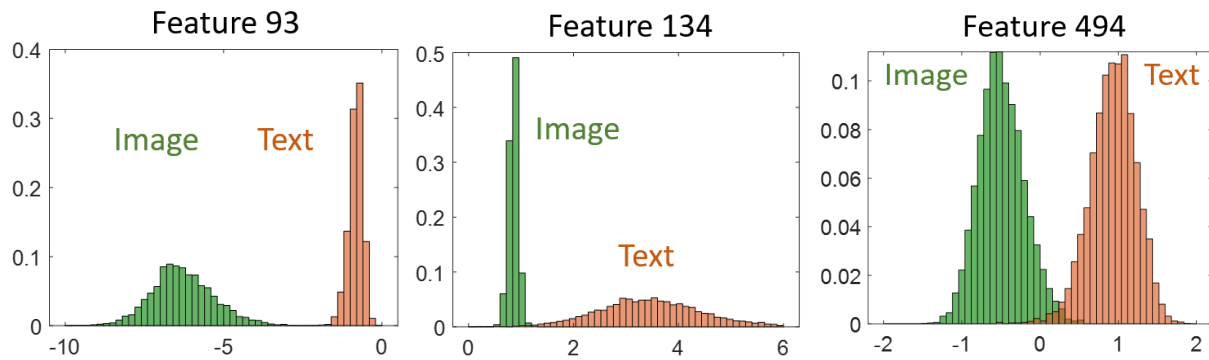


Figure 2. Enlarged plots from Section 4.

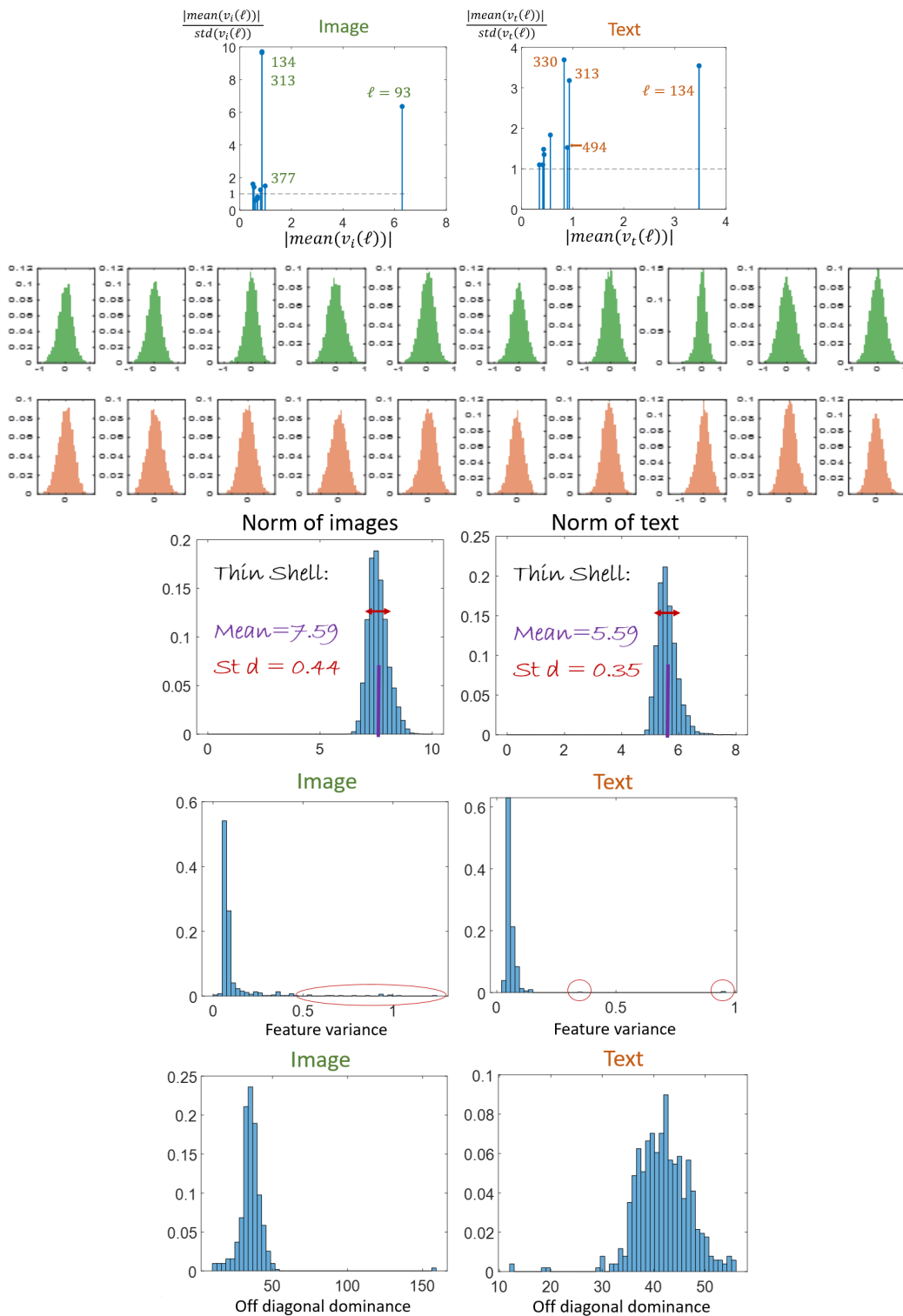


Figure 3. Enlarged plots from Section 4.

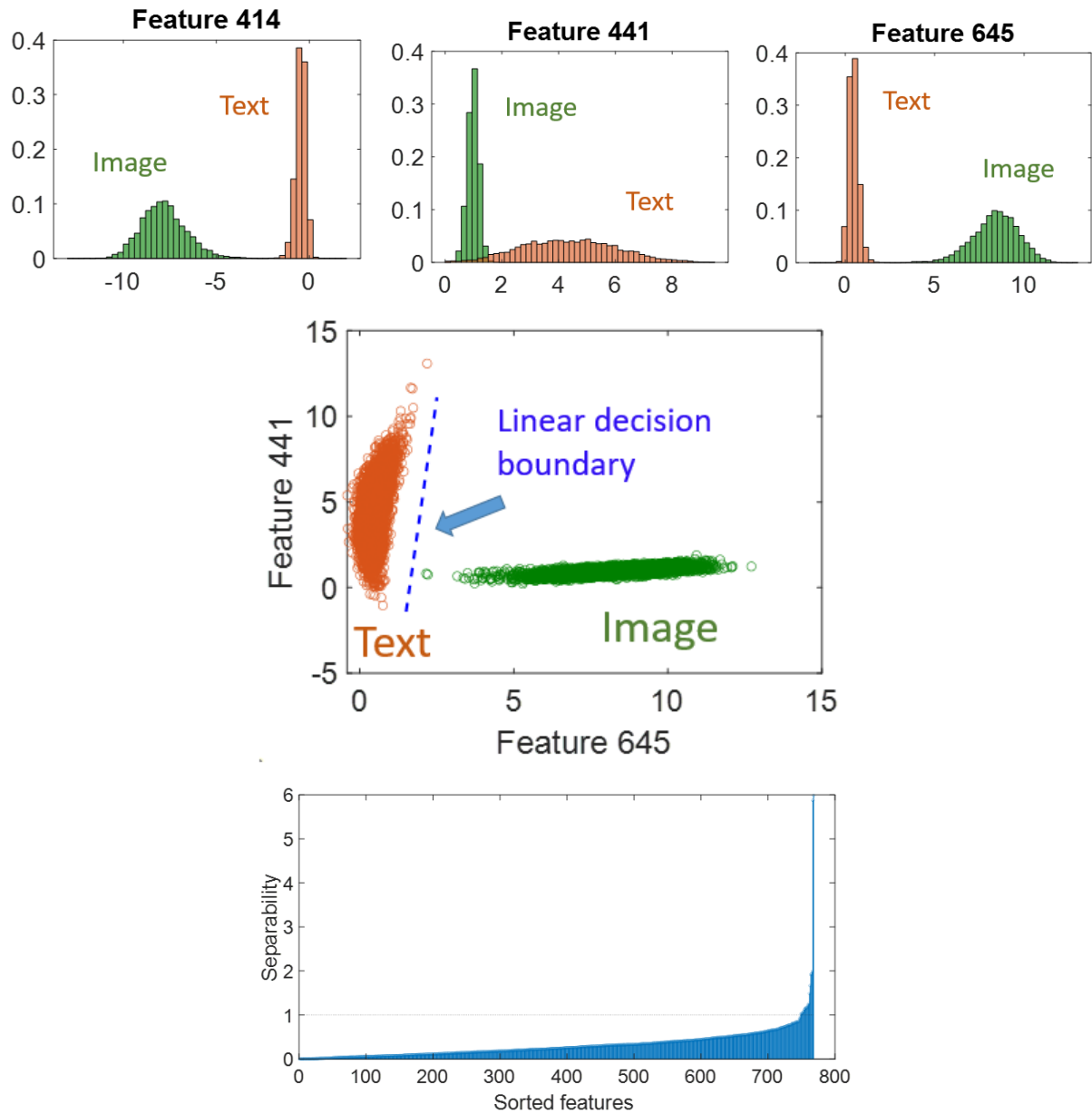


Figure 4. **Enlarged plots for CLIP embedding of $n = 768$.** There are dominant features with clearly different distribution between image and text. Both modalities can be separated (with perfect accuracy) by a linear SVM classifier based on only 2 features. With respect to separability (bottom), there are 20 features with value above 1.

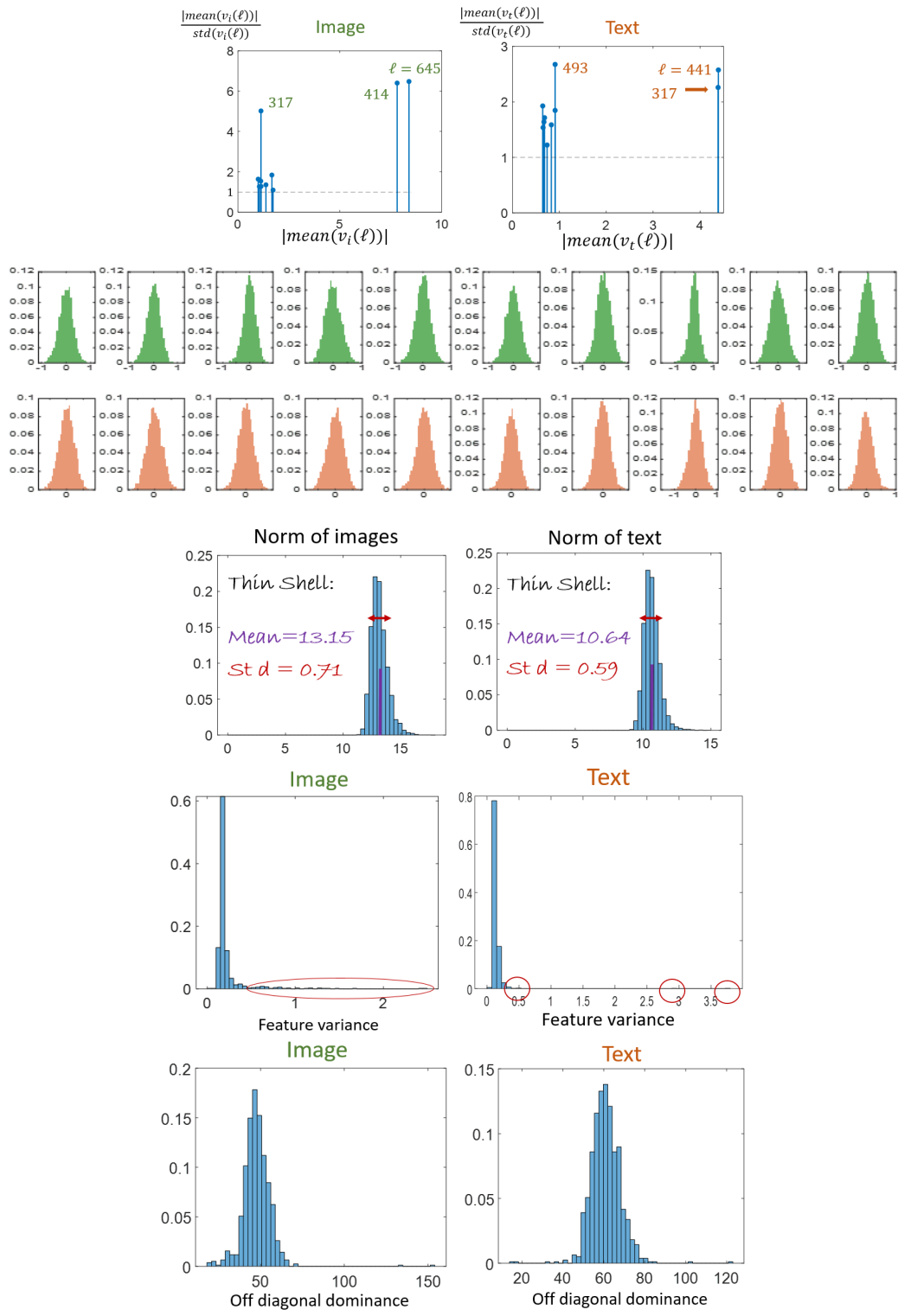


Figure 5. CLIP $n = 768$, thin shell phenomenon. We can observe similar geometry (as in the case of $n = 512$) of two tilted ellipsoids, one for each modality, not centered at the origin.



Figure 6. High and low conformity of sketches from ImageNet-R. Images with high conformity tend to be simpler and cleaner, while low-conformity images often feature complex details covered by large portions of text descriptions.



Figure 7. Conformity on ImageNet-a. It is possible that high conformity images are with more unique colors, perhaps contains people or text, whereas low conformity images tends to contain low amount of information.

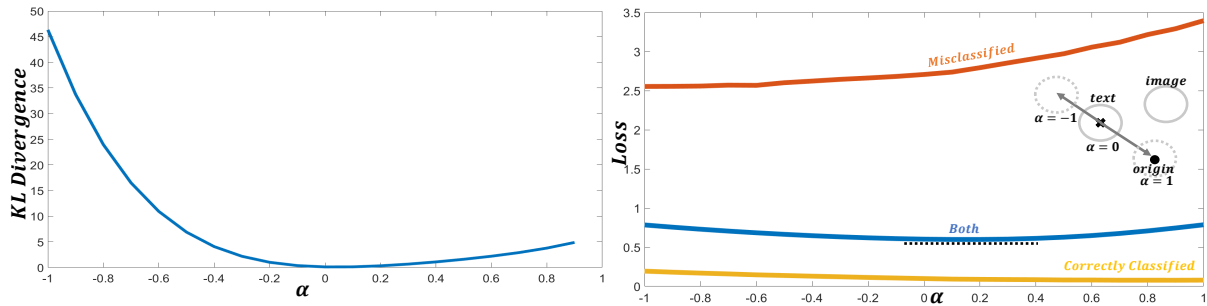


Figure 8. **Shifting text ellipsoid only.** Conformity distribution matching and loss experiments when shifting text ellipsoid only as in Eq. (3)

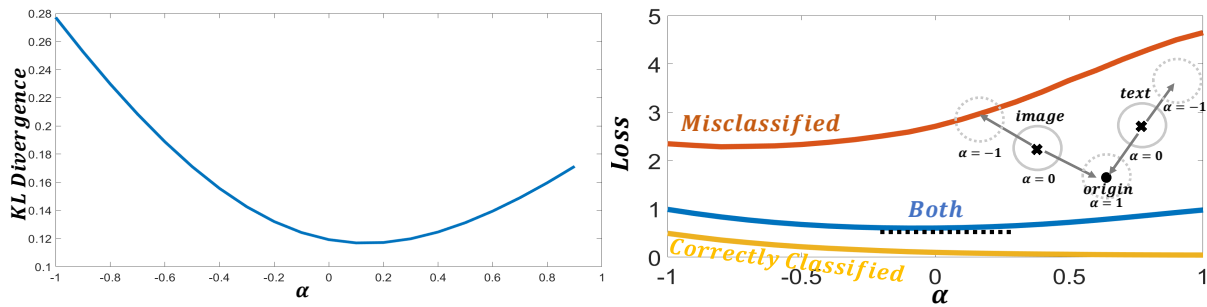


Figure 9. **Shifting both ellipsoids.** Conformity distribution matching and loss experiments when shifting both text and image ellipsoids as in Eq. (4).



Figure 10. **vSLERP lamp to vase.**

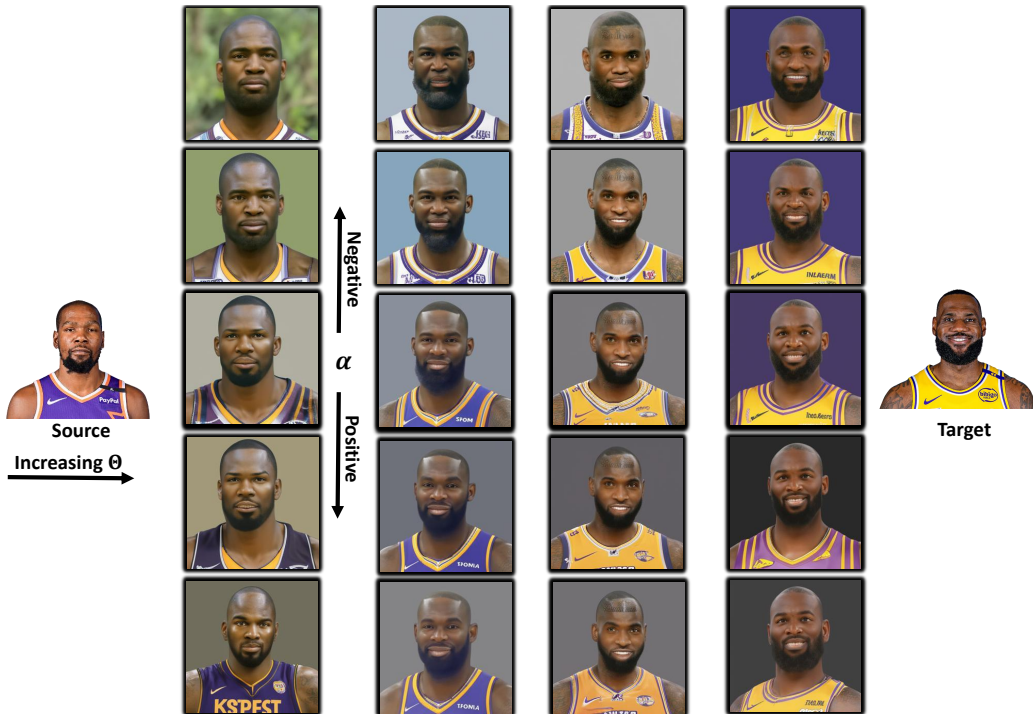


Figure 11. vSLERP Kevin Durant to LeBron James.